

Contact Pressure and Residual Strain of Resistance Spot Welding on Mild Steel Sheet Metal

Hua Zhong, Xiaodong Wan, Yuanxun Wang, and Yiping Chen

Abstract

Coupled electrical–thermal and thermo-elastic–plastic analyses were performed to analyze the behavior of the mechanical features during the resistance spot welding (RSW) process including the squeeze, heating, and hold steps, and to prepare for further structural analysis for large, complex structures with a large quantity of resistance spot welds. A two-dimensional axisymmetric thermo-elastic–plastic FEM model was developed and analyzed in the commercial FEM program, ANSYS. The analysis was based on the transient temperature field obtained from a transient electrical–thermal simulation of the RSW process conducted by the authors. The distribution and change of the contact pressure at the electrode–workpiece interface and faying surface, the residual stress, and the residual plastic strain distribution of the weldment were obtained through the analysis.

Keywords

Resistance spot welding • Temperature field
Contact pressure • Residual strain

Introduction

The resistance spot welding (RSW) process is widely used in sheet metal joining due to its advantages in welding efficiency and suitability for automation. For example, a modern vehicle typically contains 2000–5000 spot welds. Thus, the behavior of the RSW process is extremely important to the quality of the entire welding production.

During the RSW process, deformation, stress, and strain will be generated and changed in the weldment due to the electrode force and Joule heating, and residual stress and strain will retain in the weldment after welding. It is a complex process in which coupled interactions exist with electrical, thermal, mechanical, and metallurgical phenomena, and even surface behaviors. Numerous studies of the mechanical features for such a complex process have been performed on all kinds of welding conditions and materials, using both theoretical and experimental methods [5, 7, 12]. It can be concluded from these studies that spot welding failure is likely related to many parameters of the RSW process, e.g., residual stress, welding parameters, welding schedule, sheet thickness, welding gap, welding nugget size, and material properties. These parameters also affect the fatigue life of the welded joint. Results of the relative research studies show that the fatigue strength is mainly controlled by the residual stress, welding gap, and stress concentration at the notch of the welding nugget [1, 10, 14].

Recently, numerical methods have proved to be powerful tools in studying these interactions, especially the finite element analysis (FEA) method, which can deal with non-linear behaviors and complex boundary conditions. It has become the most important method for the analysis of the RSW process [8, 9, 15] developed a real-time control method in RSW and obtained direct correlations between welding nugget formation and expansion displacement of electrodes. Nied [13] developed the first FEA model for the RSW process, investigated the effect of the geometry of the electrode on the workpiece, and predicted the deformation

H. Zhong · X. Wan
School of Mechanical Science and Engineering, Huazhong
University of Science and Technology, Wuhan, 430074, China

Y. Wang (✉) · Y. Chen (✉)
School of Civil Engineering and Mechanics, Huazhong University
of Science and Technology, Wuhan, 430074, China
e-mail: wangyuanxun@hust.edu.cn

Y. Chen
e-mail: ypchen88@hust.edu.cn

H. Zhong
HangYu Aerospace Life-Support Industries Co Ltd, Xiangyang,
441002, China

and stresses. However, the developed model was restricted to elastic deformation and could not calculate the contact areas at the electrode–workpiece interface and faying surface. Therefore, many researchers developed more sophisticated FEA models that incorporate the contact status, phase changing, and coupled field effects into the simulation of RSW [3, 6, 17]. The iterative method was employed to simulate the interactions between coupled electrical, thermal, and structural fields [4, 11]. In this method, the stress field and contact status were initially obtained from the thermo-mechanical analysis, and then the temperature field was obtained from the fully coupled electrical–thermal analysis based on the contact area at the electrode–workpiece interface and faying surface. The calculated temperature field was then passed back to the thermo-structural analysis to update the stress field and contact status. The iterative method can provide the temperature field, the electric potential field, and the stress and strain distributions of the spot welding in one calculation, but the simulation of transient processes with such a methodology would probably require a large amount of computing time. On the other hand, although so many studies have been conducted, we still do not have adequate and accurate information of the RSW process due to its inherent complexity. More detailed analyses are needed of the mechanical features during the whole process of RSW.

The objective of this paper is to develop a multi-coupled method to analyze the welding deformation of the RSW process in order to reduce the computing time with the minimum loss of computing accuracy. The behavior of the mechanical features during the RSW process including the squeeze, heating, and hold steps are very important for further structural analysis for large, complex structures with a large quantity of resistance spot welds.

Model and Mesh

For the solution of the welding deformation of the RSW process in this research, an axisymmetric model was developed and solved using the FEA method based on ANSYS code. The two-dimensional axisymmetric model is illustrated schematically in Fig. 1, where x and y represent the faying surface and the axisymmetric axis, respectively. Its corresponding dimensions are $OE = HI = 1.5$ mm for two sheets of equal thickness, $OI = EH = 15$ mm for the spot welding area, $PA = FG = 5$ mm and $AG = 18$ mm for the cooling water area, $PB = 11$ mm for the radius of the electrode, $EF = 12.5$ mm, $ED = 3$ mm, $OP = 32$ mm and $\alpha = 30^\circ$, while the lower half of the model is mirror symmetric about the faying surface of the two sheet metals.

The model was meshed using three types of elements, as shown in Fig. 2. The solid elements were employed to simulate the thermo-elastic–plastic behavior of the sheets

Fig. 1 Schematic diagram for the model of RSW

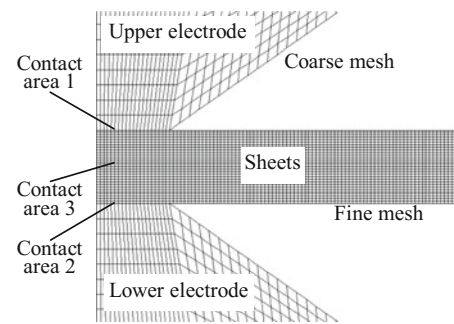
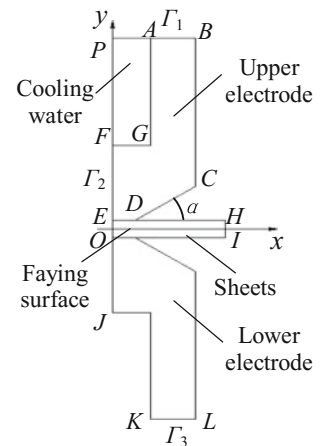


Fig. 2 Mesh generation of the developed model

and electrodes. The contact pair elements were employed to simulate the contact areas. There were three contact areas in the model. Contact areas 1 and 2 represented the electrode–workpiece interface, and contact area 3 represented the faying surface. They were all assumed to be in contact with two deformable surfaces, and these surfaces were allowed to undergo small sliding. In order to obtain reliable results, fine meshes were generated near these contact areas, while the meshes of other areas were relatively coarse.

Governing Equations and Boundary Conditions

The constitutive equations of the materials for axisymmetric transient thermal analysis based on thermo-elastic–plastic theory can be written as

$$d\{\sigma\} = [D]d\{\varepsilon\} - \{C\}dT \quad (1)$$

$$\{C\} = -[D] \left(\{\alpha\} + \frac{\partial[D]^{-1}}{\partial T} \{\sigma\} \right) \quad (2)$$

where $\{\sigma\}$ is the stress vector, $\{\varepsilon\}$ is the strain vector, $\{\alpha\}$ is the thermal expansion coefficient, and $[D]$ is the elastic–plastic matrix with $[D]=[D]_e$ in the elastic area, and $[D]=[D]_{ep}=[D]_e-[D]_p$ in the plastic area, in which $[D]_e$ is the elastic matrix and $[D]_p$ is the plastic matrix.

For the structural analysis, the stress equilibrium equation is given by

$$\nabla\sigma(r,t)+b(r,t)=0 \quad (3)$$

Where σ is the stress, b is the body force and r is the coordinate vector. For the transient thermal analysis, the following boundary conditions are specified on the surface of Γ_1 , Γ_2 , and Γ_3 (see Fig. 1).

- Γ_1 (AB): $\sigma_y = -q$, where q is the uniform pressure which can be determined according to the electrode force and the section area of the electrode.
- Γ_2 (FEOJ): $U_x = 0$, where U_x is the displacement in x direction.
- Γ_3 (KL): $U_y = 0$, where U_y is the displacement in y direction.

Welding Parameters and Material Properties

The welding parameters used in this analysis are welding current of 50 Hz, sine wave AC current of 12.2 kA, weld time of 13 cycles (0.26 s), electrode force of 3 kN, and holding time of 3 cycles (0.06 s).

Because the materials are subjected to a wide range of temperatures, most of the material properties are considered as temperature-dependent. The most important property in the analysis of the RSW process is the contact resistivity of the faying surface. The contact resistivity is a dependent function on contact pressure, temperature, and average yield strength of two contact materials. Vogler and Sheppard [16] pointed out that the contact resistance decreases as the contact pressure increases. Using a curve fitting procedure, Babu et al. [2] developed an empirical model for establishing the desired relationship of contact resistance against pressure and temperature. During the RSW process, the contact resistivity distribution influences the current density pattern, which affects the temperature field through Joule heating, while the temperature field then influences the mechanical pressure distribution through thermal expansion, related to the interface resistivity. Therefore, this is a highly non-linear problem involving the complex interaction of thermal, electrical, and mechanical phenomena. To simplify the problem, many researchers took the contact resistivity as a function of temperature [3, 6, 11, 17]. This simplification is reasonable since, firstly, the load is constant in a specified

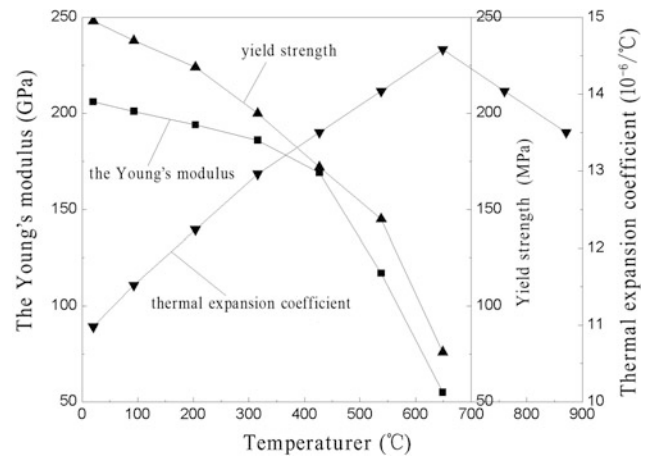


Fig. 3 Mechanical and thermal properties of the mild steel

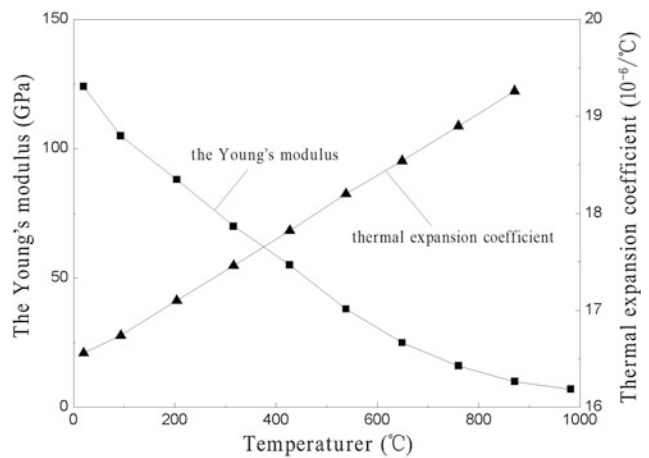


Fig. 4 Mechanical and thermal properties of the copper electrode

RSW process and, secondly, the yield strength of the materials, which determines the contact status in the contact area, is essentially influenced by temperature. With this simplification, the computing time can be reduced greatly. Therefore, in this research, the temperature-dependent contact resistance was imposed at the faying surface. The mechanical and thermal properties of both the copper electrode and mild steel sheet workpiece are shown in Figs. 3 and 4.

Thermo-Elastic-Plastic Analysis

The temperature field and its changing of the sheet metal RSW have been obtained and well discussed through the coupled electrical–thermal analysis by Hou et al. [8, 9]. Figure 5 shows the temperature-changing histories at the center of the weld nugget (point O in Fig. 1) and the center and the edge of the electrode–workpiece interface (points E

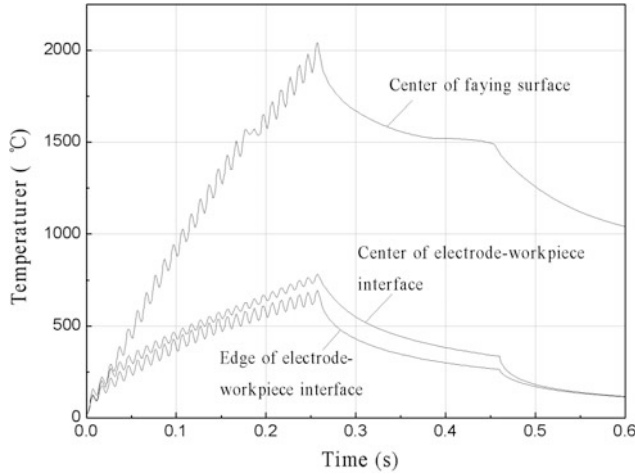


Fig. 5 Temperature-changing histories of the RSW process

and D in Fig. 1) from which we can see the changing of temperature and the heat affected zone (HAZ) during the RSW process.

For the thermo-elastic-plastic analysis, some hypotheses are cited. The mechanical properties stress and strain related with the welding temperature are linearly changed in a small time increment. Elastic stress, plastic stress, and temperature stress are separable. Strain stiffening occurs in the plastic field and obeys the theory of rheology. The Mises Yield Criterion is used for the material yield strength. The welding thermo-elastic-plastic analysis is constructed by the strain-displacement relationship or compatibility condition, stress-strain relationship or constitutive relationship, equilibrium condition, and boundary conditions. The constitutive equations of the material in the temperature field can be written as Eq. (1). In the elastic field, $[D] = [D]_e$ is the elastic matrix, and

$$\{C\} = \{C\}_e = [D]_e \left(\{\alpha\} + \frac{\partial [D]_e^{-1}}{\partial T} \{\sigma\} \right) \quad (4)$$

$\{\alpha\}$ is the thermal expansion coefficient. In the plastic field, $[D] = [D]_{ep}$, and

$$[D]_{ep} = [D]_e - [D]_e \left\{ \frac{\partial f}{\partial \sigma} \right\} \left\{ \frac{\partial f}{\partial \sigma} \right\}^T [D]_e / S \quad (5)$$

$$S = \left\{ \frac{\partial f}{\partial \sigma} \right\}^T [D]_e \left\{ \frac{\partial f}{\partial \sigma} \right\} + \left(\frac{\partial f_0}{\partial K} \right) \left\{ \frac{\partial K}{\partial \varepsilon} \right\}^T \left\{ \frac{\partial f}{\partial \sigma} \right\} \quad (6)$$

$$\{C\} = \{C\}_{ep} = [D]_{ep} \{\alpha\} + [D]_{ep} \frac{\partial [D]_e^{-1}}{\partial T} \{\alpha\} - [D]_e \frac{\partial f}{\partial \sigma} \frac{\partial f_0}{\partial T} / S \quad (7)$$

where $f(\sigma_x, \sigma_y, \dots)$ is the yield function. The material would yield at the value $f_0(\sigma_s, T, K)$ at the temperature T and the strain hardening exponential K . At loading, the consistency condition must be content, so,

$$\left\{ \frac{\partial f}{\partial \sigma} \right\}^T \{d\sigma\} = \left(\frac{\partial f_0}{\partial K} \right) \left\{ \frac{\partial K}{\partial \varepsilon} \right\}^T \{d\varepsilon\} + \frac{\partial f_0}{\partial T} dT \quad (8)$$

For any cell of the weldment, at time τ , temperature is T , force at the node is $\{F\}_e$, node displacement is $\{\delta\}$, strain is $\{\varepsilon\}$, stress is $\{\sigma\}$, and at time $\tau + d\tau$, there are $T + dT$, $\{F + dF\}_e$, $\{\delta + d\delta\}$, $\{\varepsilon + d\varepsilon\}$, $\{\sigma + d\sigma\}$. Using the virtual displacement principle, we can obtain

$$\begin{aligned} \{d\delta\}^T \{F + dF\}_e &= \iint_{\Delta V} \{d\delta\}^T [B]^T (\{\sigma\} + [D]\{d\varepsilon\} - \{C\}dT) dV \\ &= \{d\delta\}^T \iint_{\Delta V} [B]^T (\{\sigma\} + [D]\{d\varepsilon\} - \{C\}dT) dV \end{aligned} \quad (9)$$

It is equilibrium at time τ , so,

$$\{F\}_e = \iint_{\Delta V} [B]^T \{\sigma\} dV \quad (10)$$

Then, Eq. (1) can be expressed as

$$\{dF\}_e = \iint_{\Delta V} [B]^T ([D]\{d\varepsilon\} - \{C\}dT) dV \quad (11)$$

or written as

$$\{dF\}_e + \{dR\}_e = [K]_e \{d\delta\} \quad (12)$$

where the original strain equivalent node force is

$$\{dR\}_e = \iint_{\Delta V} [B]^T \{C\} dT dV \quad (13)$$

Cell stiffness matrix is

$$[K]_e = \iint_{\Delta V} [B]^T [D] [B] dV \quad (14)$$

Given the different $[D]$ and $\{C\}$ according to the elastic or plastic state, the equivalent node load and stiffness matrices can be obtained. Then, posting them to the general stiffness matrix and the general load vector, the algebra equations of the node displacement can be obtained by

$$[K] \{d\delta\} = \{dF\} \quad (15)$$

where

$$[K] = \sum [K]_e \quad (16)$$

$$\{dF\} = \sum (\{dF\}_e + \{dR\}_e) \quad (17)$$

For welding problems, $\sum \{dF\}_e$ is often zero, then,

$$\{dF\} = \sum \{dR\}_e \tag{18}$$

From the algebra equations (15), the node displacement can be obtained, and then the node stress can be obtained through the constitutive equations.

To correctly load the temperature field, the FEA model and mesh in the thermo-elastic-plastic analysis are identical with those in the temperature field analysis as shown in Fig. 1. But the boundary conditions and the property of the mesh cells must be changed correspondingly. For the plastic material of the mild steel and copper electrode, the double linear thermo-elastic strengthen material model is adopted, and the physical equations are

$$\begin{cases} \varepsilon = \frac{\sigma}{E} & (|\sigma| \leq \sigma_s) \\ \varepsilon = \frac{\sigma}{E} + (|\sigma| - \sigma_s) \left(\frac{1}{E'} - \frac{1}{E}\right) \text{sign } \sigma & (|\sigma| > \sigma_s) \end{cases} \tag{19}$$

in which the material mechanical parameters, including the Young’s modulus E , shear modulus E' , and yield strength σ_s , which changed with temperature, are shown in Figs. 3 and 4. The shear modulus E' is taken as 1/10 of the Young’s modulus E at corresponding temperature.

The electrode force was loaded at the contact surface (EH and OI in Fig. 1) of the electrode and the mild steel sheets as a uniform load. The load boundary condition was $\sigma_y = -q$, where q was the load intensity obtained by the contact pressure. Loading the temperature field at the corresponding time as the node body

load, the APDL (analysis parametric design language) loop language of ANSYS was used in the loading process.

Results and Discussion

Contact Pressure

The contact pressures at the faying surface of the two sheet metals and the electrode-workpiece interface can be divided into three steps. Figure 6 shows the contact pressures on the faying surface of the two sheet metals at different heating cycles. During the squeeze step (marked as cycle 0), a maximum contact pressure of 83 MPa was attained near the edge of contact area, and the pressure at the faying surface was a little changed. As the heating cycles started (electrifying), the pressure near the edge of the contact area was decreased, while the pressure at the center of the contact area increased quickly. Cycle 1 to cycle 3 compose the second step. At cycle 3, the maximum contact pressure at the center of the faying surface of the two sheet metals reached 155 MPa, with a contact area radius of 3 mm. Then, the pressure near the edge of the contact area started to increase, became and kept larger than that of the center of the contact area during the consequent cycles at the third step from cycle 4 to cycle 8. The peak value of 168 MPa appeared at cycle 5, with the a contact area radius of 3.1 mm. At the same time, the location of the maximum pressure value moved outward

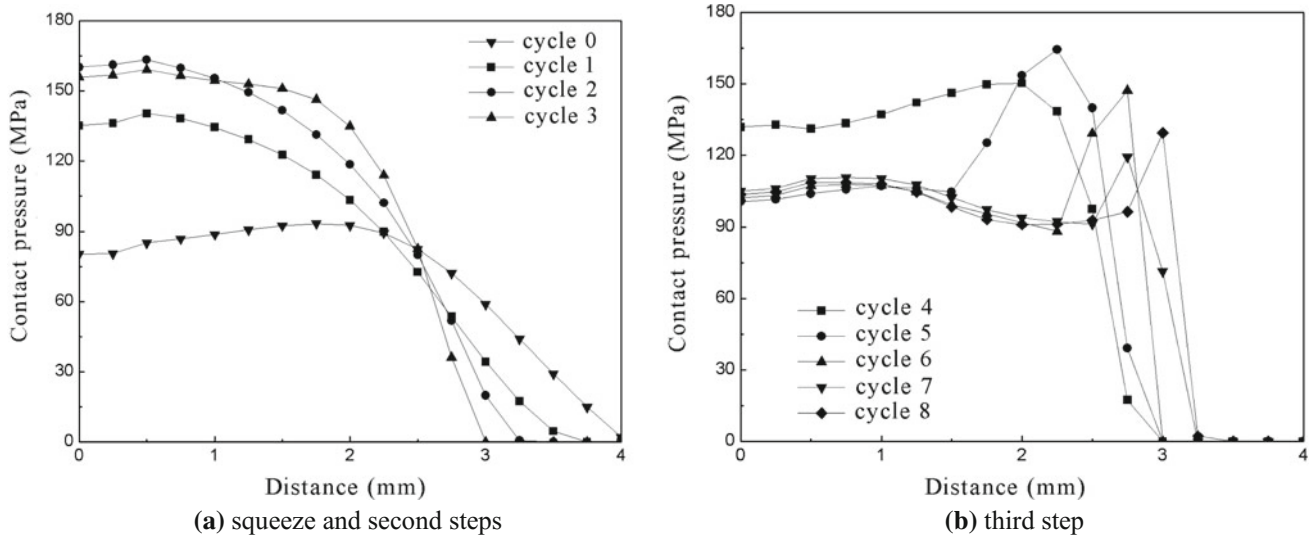


Fig. 6 Contact pressure at the faying surface

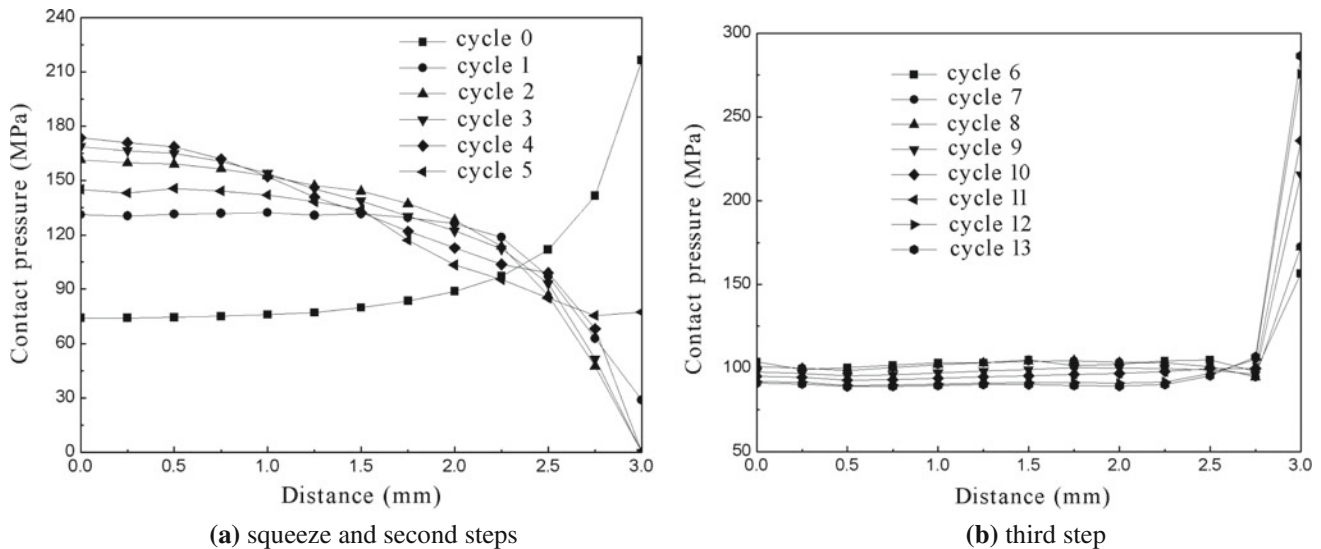


Fig. 7 Contact pressure at the electrode-workpiece interface

from the contact area. The high contact pressure near the edge of the contact area is a benefit to the RSW process because it can prevent liquid metal expulsion during welding. The contact area on the faying surface of the two sheet metals was nearly constant during the heating cycles. The radius of the contact area was varied in a narrow range from 3–3.5 mm.

The distributions and change of the contact pressure due to the thermal expansion of the RSW welding joint and the material properties were subjected to a wide range of temperatures. At the second step, the temperature at the center of the faying surface of the two sheet metals was increased rapidly and the temperature near the edge was quite low, so the thermal expansion of the material in the center of the faying surface was much bigger than that near the edge. The contact pressure in the center of the faying surface was larger. At the third step, the Young's modulus and yield strength of the material at the center of the faying surface decreased obviously with the increase of the temperature.

The contact pressure distributions on the electrode-workpiece interface are shown in Fig. 7. Obviously, it has a different pattern from that on the faying surface of the two sheet metals. During the squeeze step (cycle 0), the pressure was relatively uniform near the center of the contact area but very steep at the edge of the contact area. As the heating cycles started, the pressure profile changed. The pressure near the center of the contact area increased while the pressure at the edge of the contact area decreased quickly. Since the temperature at the center of the contact area increased quickly, the material along the axisymmetric axis

expanded, while the temperature at the edge of the contact area was still low and the material was unchanged. This status was kept for 4 cycles, and then another change occurred. The distribution pattern became similar to that of the squeeze step. This is probably because the temperature near the center of the contact area became so high that the Young's modulus of the material decreased, while the temperature at the edge of the contact area increased and led to thermal expansion. The contact pressure distribution was kept on this status up to the end of holding step, which means the electrode edge was kept working under large stress. In other words, there was a stress concentration at the edge of the electrode, which could be the vital cause for the abrasion of the electrode tip.

Residual Stress

The stress field in the weldment during the RSW process is very complex. The normal stress σ_y has an important influence on the form of the weld nugget. Figure 8 shows the distribution of normal stress σ_y at the squeeze and weld nugget forming steps. It can be seen that there was mainly compressive stress in the contact area, and the maximum stress was about 172 MPa at the edge of the electrode-workpiece interface. Figure 8b, c show the distribution of normal stress σ_y at cycle 9 and cycle 13, when the weld nugget started to form and completely formed (the end of holding step). The stress field became more complex due to the generation of thermal stress.

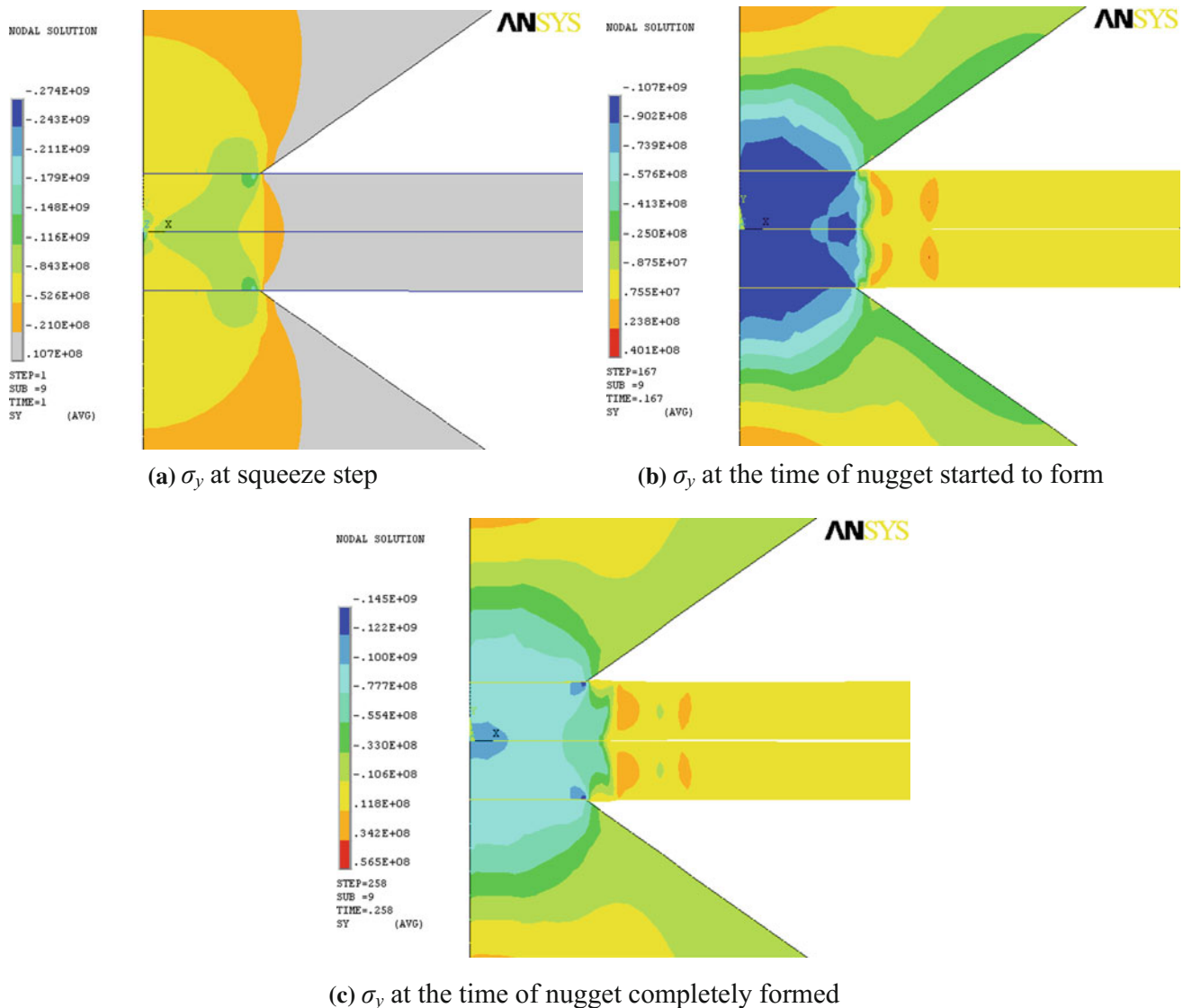


Fig. 8 Normal stress σ_y in the weldment during the RSW process

Residual Plastic Strain and Welding Deformation

The distribution and change of the strain, especially the plastic strain, is very important to the residual stress and deformation of the weldment. The strain field in the weldment during the RSW process is also very complex. The welding residual stress is produced in the welded joint as a result of plastic deformation caused by non-uniform thermal expansion and contraction due to non-uniform temperature distribution in the welding process. Figure 9 shows the residual plastic strain of the weldment in radial and normal orientation after welding. It can be seen that the radial residual plastic strain is mostly compression strain and the normal strain is tension strain on the contrary. The maximum of the residual plastic strain occurred near the edge of

the contact area through the thickness of the sheets. Comparing Fig. 10, the distribution of residual plastic strain of the weldment in radial and normal orientation at the highest temperature after RSW welding, we can give the following discussion. During the RSW process, the material in the center part of the welding joint expanded with electrifying and heating up, but embarrassed by the material around in the radial orientation. So, a larger compression plastic strain was produced as shown in Fig. 10a. The maximum radial compression plastic strain was about 0.063955 at the highest temperature after welding.

Embarrassed in the radial orientation, the deformation of the material was turned to the normal orientation during the RSW process. Compressed by the electrode pressure in the radial orientation (but the pressure was less than the

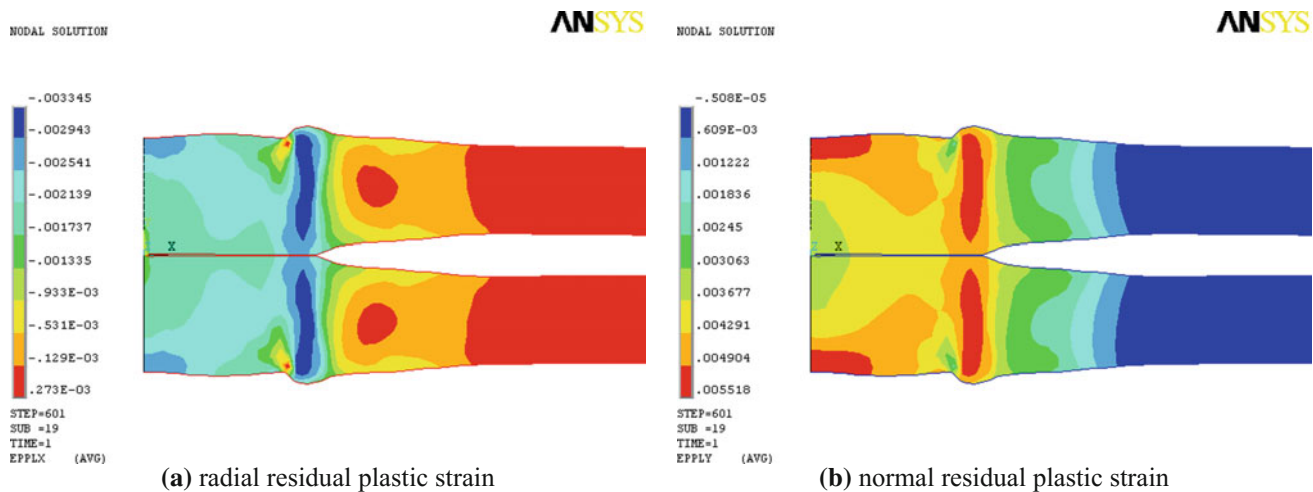


Fig. 9 Residual plastic strain of the weldment after welding

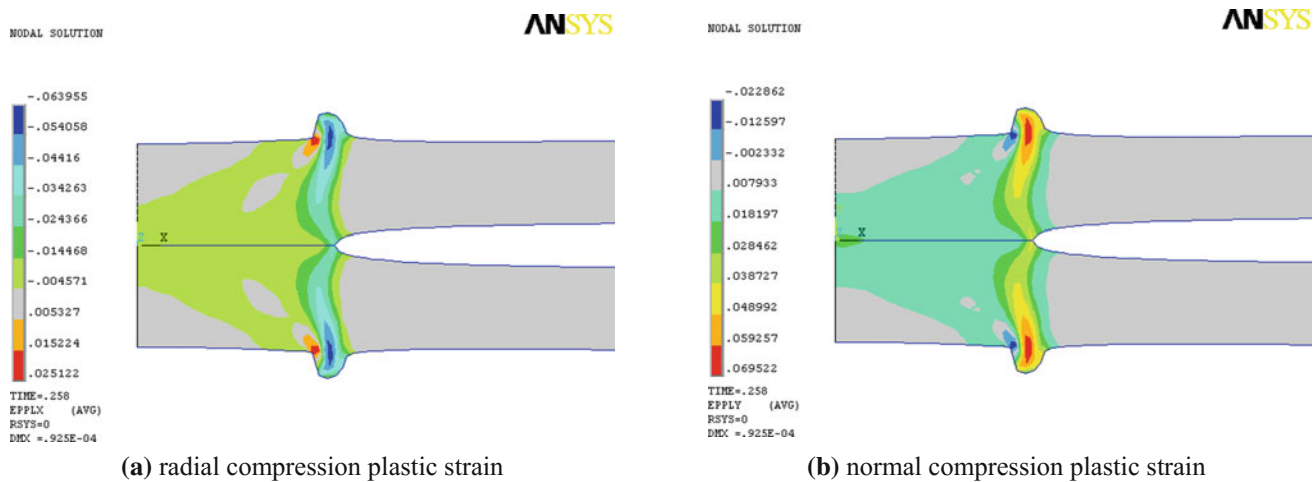


Fig. 10 Residual plastic strain of the weldment at highest temperature after welding

resistance of the thermal expansion of the material of the welding joint), the normal dimension increased and the normal tension plastic strain was produced. The material near the edge of the electrode was extruded and larger tension plastic strain was produced as shown in Fig. 10b. The maximum normal tension plastic strain was about 0.069522 at the highest temperature after welding.

Once electrifying after welding stopped, compression of the material started. Embarrassed by the material around in the radial orientation, tension plastic strain was produced and the radial compression plastic strain could be counteracted partly but not completely, so the residual compression plastic strain remained. Figure 9a shows that the residual compression plastic strain was only about 0.003345; most of the residual compression plastic strain was eliminated. In the normal orientation, compression plastic strain was produced by the electrode pressure, most of the tension plastic strain

was eliminated, and residual tension plastic strain remained. Figure 9b shows that the residual tension plastic strain was about 0.005518.

Conclusions

The determinations of the contact pressure at the faying surface and electrode–workpiece interface are important aspects of the numerical analysis. The distributions of the contact pressure at the faying surface are very important during the RSW process, because they determine the distribution of the electric resistance. The contact resistance distribution influences the current density pattern, which affects the temperature field through Joule heating, while the temperature field then influences the mechanical behavior of the weldment. The distributions of the contact pressure at the

electrode–workpiece interface have little influence on the temperature field, however, they have great influence on the useful life of the electrode.

The deformation of the weldment is produced due to the residual plastic strain. The residual plastic strain and the welding deformation are symmetrical if the two sheet workpieces have equal thickness. Research studies show that the symmetrical residual plastic strain has a very small influence on the deformation of the welding structure.

Acknowledgments Yuanxun Wang: Project supported by the financial support from the National Natural Science Foundation of China (11072083).

References

1. Adib H, Gilgert J, Pluvinage G (2004) Fatigue life duration prediction for welded spots by volumetric method. *Int J Fatigue* 26:81–94
2. Babu SS, Santella M, Feng LZ, Riemer BW, Cohron JW (2001) Empirical model of effects of pressure and temperature on electrical contact resistance of metals. *Sci Technol Weld Join* 6:126–132
3. Browne DJ, Chandler HW, Evans J, Wen TJ (1995) Computer simulation of resistance spot welding in aluminum: part I. *Weld J* 74:339s–344s
4. Chang BH, Li M, Zhou VY (2001) Comparative study of small scale and ‘large scale’ resistance spot welding. *Sci Technol Weld Join* 6:273–280
5. Chao YJ (2003) Ultimate strength and failure mechanism of resistance spot weld subjected to tensile, shear, or combined tensile/shear loads. *J Eng Mater Technol Trans ASME* 125:125–132
6. Cho HS, Cho YJ (1989) A study of the thermal behavior in resistance spot welds. *Weld J* 68:236s–244s
7. Deng X, Chen W, Shi G (2000) Three-dimensional finite element analysis of the mechanical behavior of spot welds. *Finite Elem Anal Des* 35:17–39
8. Hou ZG, Kim IS, Wang YX, Li CZ, Chen CY (2007) Finite element analysis for the mechanical features of resistance spot welding process. *J Mater Process Tech* 185:160–165
9. Hou ZG, Wang YX, Li CZ, Chen CY (2006) A multi-coupled finite element analysis of resistance spot welding process. *Acta Mech Solida Sin* 19:86–94
10. Kang H, Barkey ME, Lee Y (2000) Evaluation of multiaxial spot weld fatigue parameters for proportional loading. *Int J Fatigue* 22:691–702
11. Khan JA, Xu L, Chao Y (1999) Prediction of nugget development during resistance spot welding using coupled thermal–electrical–mechanical model. *Sci Technol Weld Join* 4:201–207
12. Lin SH, Pan J, Tyan T, Prasad P (2003) A general failure criterion for spot welds under combined loading conditions. *Int J Solids Struct* 40:5539–5564
13. Nied HA (1984) The finite element modeling of the resistance spot welding process. *Weld J* 63:123s–132s
14. Pan N, Sheppard S (2002) Spot welds fatigue life prediction with cyclic strain range. *Int J Fatigue* 24:519–528
15. Tsai CL, Dai WL, Dickinson DW, Papritan JC (1991) Analysis and development of a real-time control methodology in resistance spot welding. *Weld J* 70:339s–351s
16. Vogler M, Sheppard S (1993) Electrical contact resistance under high loads and elevated temperatures. *Weld J* 72:231s–238s
17. Yeung KS, Thornton PH (1999) Transient thermal analysis of spot welding electrodes. *Weld J* 78:1s–6s